Centrality dependence of mapping the hydrodynamic response to the initial geometry in heavy-ion collisions

Jinghua Fu*

Institute of Particle Physics, Central China Normal University, Wuhan 430079, People's Republic of China and Key Laboratory of Quark & Lepton Physics (CCNU), Ministry of Education, People's Republic of China

(Received 2 April 2015; revised manuscript received 15 July 2015; published 10 August 2015)

Event-by-event correlations between v_n and $\varepsilon_{m,n}$ for different collision centralities are studied with hydrodynamics. For the more central collisions v_n is better correlated with $\varepsilon_{m,n}$ defined with relatively larger radial weight power m, like $m = n + 1$. For the more peripheral collisions, v_n prefers $\varepsilon_{m,n}$ with relatively smaller m, like $m = n - 1$. When the fluid viscosity is large, v_n is better correlated with $\varepsilon_{m,n}$ with large m. For the most central collisions and for odd harmonics, since anisotropy is solely due to fluctuations, the scaled probability distributions of $\varepsilon_{m,n}$ are universal. For noncentral collisions, the scaled probability distributions of $\varepsilon_{m,2}$ with different radial weight power m deviate from one another. $\varepsilon_{m,2}$ defined with smaller m has a wider scaled distribution and a larger scaled standard deviation, and is more consistent with the scaled v_2 distribution after hydrodynamic evolution in peripheral collisions. Hadronic rescattering widens the v_2 distribution in noncentral collisions, which contributes to the observed inconsistency between $p(v_2)$ and $p(\varepsilon_2)$ distributions.

DOI: 10.1103/PhysRevC.92.024904 PACS number(s): 25.75.Ld, 24.10.Nz

I. INTRODUCTION

Recent data from ultrarelativistic heavy-ion collisions at the Relativistic Heavy Ion Collider (RHIC) and the Large Hadron Collider (LHC) strongly support the dynamical picture according to which the produced soft hadronic distributions in transverse momentum, azimuthal orientation, centrality, and particle species are determined by the fluid dynamic response to fluctuating initial conditions [1,2]. Relativistic hydrodynamics has been able to successfully describe the large azimuthal momentum anisotropies observed in heavy-ion collisions, which suggests the quark gluon plasma as a strongly interacting fluid with one of the smallest shear viscosity to entropy density ratios ever observed [3].

Quantitatively, the particle azimuthal distribution is characterized in terms of the coefficients v_n of the Fourier expansion of the invariant triple differential distributions [4]:

$$E\frac{d^3N}{d^3p} = \frac{1}{2\pi}\frac{d^2N}{p_T dp_T dy}\left[1 + \sum_{n=1}^{\infty} 2v_n \cos\left[n(\phi - \Psi_n)\right]\right], \tag{1}$$

with

$$\vec{v}_n(y, p_T) = v_n e^{in\Psi_n}(y, p_T) = \frac{\int d\phi e^{in\phi} E\frac{d^3N}{d^3p}}{\int d\phi E\frac{d^3N}{d^3p}}, \tag{2}$$

where ϕ is the transverse momentum azimuthal angle.

The study of strongly coupled matter with hydrodynamics requires that one supplies a set of initial conditions, then evolves them through ideal or viscous hydrodynamics, and finally computes the particle emission [5,6]. One of the main features of the hydrodynamical description of the expansion is that, if the system has an approximate boost invariance near midrapidity, and if the initial transverse flow and initial viscous tensor are negligible, the momentum distribution of particles at the end of the evolution is determined by the initial transverse energy density profile $\rho(r,\phi)$.

The initial anisotropy is generally quantified in terms of the participant eccentricity:

$$\vec{\varepsilon}_{m,n} = \varepsilon_{m,n} e^{in\Phi_{m,n}} = -\frac{\int r dr d\phi\, r^m e^{in\phi}\rho(r,\phi)}{\int r dr d\phi\, r^m \rho(r,\phi)}, \tag{3}$$

where $r = \sqrt{x^2 + y^2}$ and ϕ is now the spatial azimuthal angle. In Eq. (3) r^m indicates a radial weight of the integral, and the choice of the radial weight power m might be different.

The earliest standard eccentricity [7],

$$\varepsilon_{\rm std} = \frac{\langle y^2 - x^2\rangle}{\langle y^2 + x^2\rangle}, \tag{4}$$

and later participant eccentricity [8],

$$\varepsilon_{\rm part} = \frac{\sqrt{(\langle y^2\rangle - \langle x^2\rangle)^2 + 4\langle xy\rangle^2}}{\langle y^2 + x^2\rangle}, \tag{5}$$

have r^2 weight with $m = 2$. When first generalized to the third harmonic, the r^2 weight was kept [9]. Shortly after that, Teaney and Yan [10] introduced a cumulant expansion to parametrize possible initial conditions and suggested weighting the coefficients with the nth power of r:

$$\varepsilon_{n,n} e^{in\Phi_{n,n}} = \varepsilon_n e^{in\Phi_n} = -\frac{\int r dr d\phi\, r^n e^{in\phi}\rho(r,\phi)}{\int r dr d\phi\, r^n \rho(r,\phi)}. \tag{6}$$

This definition of $\vec{\varepsilon}_{n,n}$ (often denoted simply as $\vec{\varepsilon}_n$) has a natural interpretation as the lowest momentum mode of a Fourier transform of the initial transverse density [10]. It has been shown that $\vec{\varepsilon}_n$ as defined in Eq. (6) generally gives the best estimator of $\vec{v}_n$ [11], and it is widely in use now. More recently, new methods based on a two-dimensional Fourier expansion in polar coordinate space have been proposed [12,13], which order fluctuating radial modes more explicitly in terms of

*fujh@mail.ccnu.edu.cn

functions of increasingly smaller radial resolution scale and naturally include all powers of r in the expansion.

The statistical properties of anisotropic flow are now precisely known [14]. The ATLAS Collaboration has analyzed the full probability distribution of v_2, v_3, and v_4 in Pb + Pb collisions for several centrality windows [15]. These distributions are useful to disentangle the size of fluctuations in the initial energy density profiles.

Generally, we assume that v_n in a given event is determined by linear response to the initial anisotropy, $v_n = \kappa_n \varepsilon_n$, where κ_n is a response coefficient that does not fluctuate event to event [16]. The fluctuations of v_n for $n = 2$ and 3 are due to fluctuations of the initial anisotropy ε_n in the corresponding harmonic. The problem is that the shape of the $p(\varepsilon_2)$ distributions from various initial geometry models cannot be tuned to agree with that of the $p(v_2)$ distributions across the full centrality range. It has been observed that the v_n distributions after hydrodynamic evolution are slightly wider than the initial ε_n distributions, and this widening appears to be somewhat stronger in peripheral than in central collisions [1,14,15,17,18]. That is, in peripheral collisions, $p(\varepsilon_2)$ always falls faster than $p(v_2)$ in the tail of the distributions.

As a possible explanation, a recent hydrodynamic model calculation [14,19] suggests that the response coefficient $k_2 = v_2/\varepsilon_2$ is not constant across the full ε_2 range, but increases slightly at large ε_2; hence the $p(v_2)$ distribution is expected to decrease more slowly than the $p(\varepsilon_2)$ distribution.

To better understand the relations between $p(v_n)$ and $p(\varepsilon_n)$ distributions, in this paper, I study the event-by-event correlation between the initial state anisotropies $\vec{\varepsilon}_{m,n}$ defined with different radial weight power m and the hydrodynamic response $\vec{v}_n$, and their probability distributions $p(\varepsilon_{m,n})$ and $p(v_n)$ for different collision centralities. A clear centrality dependence for better correlation between $\varepsilon_{m,n}$ and v_n is observed, and this centrality dependence provides a possible explanation for the faster falling of the tail of the $p(\varepsilon_n)$ distribution than the $p(v_n)$ distribution in peripheral collisions. Because the higher-order harmonics are coupled nonlinearly with the lower-order harmonics [11], the analysis concentrates on the second and third harmonics.

The hydrodynamic model used for this analysis is described briefly in Sec. II. Section III A presents the analysis of the event-by-event correlation between the initial condition and the flow anisotropy, while Sec. III B shows the results of their probability distributions. The reason for the different fluctuation behaviors observed for different collision centralities is explained in Sec. III B 1. The influence of hadronic rescattering on the probability distribution of v_n is discussed in Sec. III B 2.

II. METHODOLOGY

The iEBE-VISHNU code package has been used to perform event-by-event simulations for Pb + Pb collisions at $\sqrt{s} = 2.76\,A$ TeV with viscous hydrodynamics [5]. To explore the sensitivity to model uncertainties in the initial state, two sets of initial conditions are obtained from the Monte-Carlo Glauber (MC-Glauber) and Monte-Carlo KLN (MC-KLN) models [20]. The centrality classes are determined according to the number of wounded nucleons with additional requirements on the initially produced total entropy in the transverse plane [5]. Model parameters were tuned to reproduce the p_T spectra and elliptic flows of unidentified charged particles and identified hadrons [21]. This results in a specific shear viscosity of $\eta/s = 0.08$ for the MC-Glauber initial conditions and a larger value of $\eta/s = 0.2$ for the MC-KLN initial conditions. The lattice QCD and hadron resonance gas-based equation of state $s95p$-PCE-v0 [22] has been used with chemical freeze-out at temperature $T_{\rm chem} = 165$ MeV. The hadron spectra are calculated with the Cooper-Frye freeze-out procedure [23] using the decoupling temperature $T_f = 120$ MeV. Strong decay contributions from all hadron resonances with masses up to 2.25 GeV are included.

III. RESULTS

In this work I consider Pb + Pb collisions at $\sqrt{s} = 2.76\,A$ TeV. All the results shown in this paper are for positively charged pions. For every centrality class, a total of 2000 events were evolved from each of the two initial state models. The Fourier coefficients and the initial-state anisotropies were calculated according to Eqs. (2) and (3), respectively.

A. Correlations

It has been shown that the second and third Fourier coefficients have a strong event-by-event linear correlation to the initial geometry of the collision [24]. Here I study whether this correlation depends on the different r^m weights in the definition of $\vec{\varepsilon}_{m,n}$ for different collision centralities. Because it has been known that $\vec{\varepsilon}_n$ with $m = n$ as defined in Eq. (6) generally gives the best estimator of $\vec{v}_n$ [11], I concentrate on values of m around $m = n$. Specifically I first choose $m = n - 1$, n, and $n + 1$. For the second harmonic $n = 2$, m is first chosen as $m = 1$, 2, and 3. The event-by-event correlations between $\varepsilon_{(1,2,3),2}$ and v_2 for the most central 0%–5%, midcentral 20%–30%, and peripheral 50%–60% collision centralities with MC-Glauber and MC-KLN initializations are shown in Fig. 1.

To quantify the event-by-event linear correlation between the harmonics $\vec{v}_n$ and $\vec{\varepsilon}_{m,n}$, a natural choice is the linear correlation coefficient between them. Two slightly differently defined linear correlation coefficients have been introduced in previous publications [24,25]:

$$c(\varepsilon_{m,n}, v_n) = \left\langle \frac{(\varepsilon_{m,n} - \langle \varepsilon_{m,n} \rangle)(v_n - \langle v_n \rangle)}{\sigma_{\varepsilon_{m,n}} \sigma_{v_n}} \right\rangle, \tag{7}$$

and

$$Q_n(\varepsilon_{m,n}, v_n) = \frac{\mathrm{Re}\langle \vec{v}_n \vec{\varepsilon}^{\,*}_{m,n} \rangle}{\sqrt{\langle |\vec{v}_n|^2 \rangle \langle |\vec{\varepsilon}_{m,n}|^2 \rangle}}. \tag{8}$$

It is easy to see that $c(\varepsilon_{m,n}, v_n)$ considers mainly the magnitude deviation and correlation, while $Q_n(\varepsilon_{m,n}, v_n)$ defines the correlation between two vectors. For the second and third harmonics, $Q_n(\varepsilon_{m,n}, v_n)$ becomes explicitly

$$Q_2(\varepsilon_{m,2}, v_2) = \frac{\langle v_2 \varepsilon_{m,2} \cos 2(\Psi_2 - \Phi_{m,2}) \rangle}{\sqrt{\langle v_2^2 \rangle \langle \varepsilon_{m,2}^2 \rangle}} \tag{9}$$

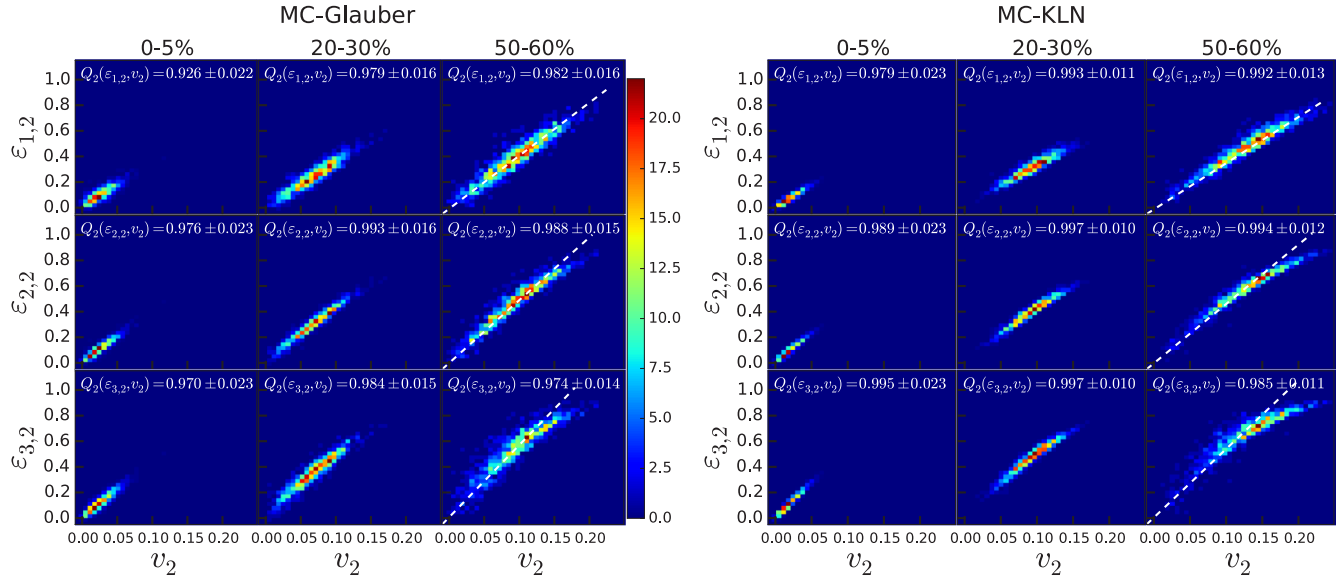

FIG. 1. (Color online) The event-by-event correlations between $\varepsilon_{1,2}$, $\varepsilon_{2,2}$, and $\varepsilon_{3,2}$ and v_2 for the centrality classes 0%–5%, 20%–30%, and 50%–60% with MC-Glauber (left) and MC-KLN (right) initializations. The dashed lines are to guide the eyes, not a fit.

and

$$Q_3(\varepsilon_{m,3},v_3)=\frac{\langle v_3\varepsilon_{m,3}\cos 3(\Psi_3-\Phi_{m,3})\rangle}{\sqrt{\langle v_3^2\rangle\langle\varepsilon_{m,3}^2\rangle}}. \qquad (10)$$

The correlation functions $c(\varepsilon_{m,n},v_n)$ and $Q_n(\varepsilon_{m,n},v_n)$ are bounded by $[-1,1]$. Larger values, closer to 1, indicate better linear correlations. $c(\varepsilon_{m,n},v_n)$ and $Q_n(\varepsilon_{m,n},v_n)$ give similar results. In the figures, the values and statistical errors of $Q_n(\varepsilon_{m,n},v_n)$ are shown.

From Fig. 1, one can see that, for all three centralities and for both initializations, $\varepsilon_{2,2}$ gives a good measure of v_2, as expected. At the same time one sees a centrality dependence for better correlation between $\varepsilon_{m,2}$ and v_2. For the most central 0%–5% collisions v_2 has better correlation with the larger radial power weighted $\varepsilon_{4,2}$ compared with $\varepsilon_{1,2}$, while for the more peripheral 50%–60% centrality class v_2 has better correlation with the smaller radial power weighted $\varepsilon_{1,2}$ compared with $\varepsilon_{4,2}$. That is, central collisions favor a relatively larger radial weight power, while peripheral collisions favor a relatively smaller radial weight power. A larger radial weight power m gives more weight to those initial energy densities that are located at larger radius r. This centrality dependence on radial weight power m indicates that v_2 is driven more by the outer layers of the fireball for central collisions, and driven more by the inner layers of the fireball for peripheral collisions, which is consistent with previous observations [11].

Because a larger specific shear viscosity of $\eta/s=0.20$ is used for the MC-KLN initialization events, better linear correlations between $\varepsilon_{m,2}$ and v_2 are obtained [24]. This larger shear viscosity also makes v_2 better correlated with the larger radial power weighted $\varepsilon_{3,2}$ for the most central 0%–5% and midcentral 20%–30% collisions, better than with $\varepsilon_{2,2}$. That is because the larger viscous effects further damp small-scale structure in the initial condition.

The response coefficient $k_2=v_2/\varepsilon_2$ is not constant across the full ε_2 range for the peripheral 50%–60% centrality class as shown in Fig. 1. k_2 increases slightly at large ε_2. The dashed lines in Fig. 1 are to guide the eyes; they are not a fit. The increase of k_2 dependences on the radial weight power used in defining $\varepsilon_{m,2}$. A larger m leads to stronger increasing of k_2. For $m=1$, $v_2/\varepsilon_{1,2}$ is approximately constant. Note that I have used v_2 as the x axis and $\varepsilon_{m,2}$ as the y axis, which is generally the other way in many of the other publications.

The results for the event-by-event third harmonic flow and eccentricity correlation from the MC-Glauber and MC-KLN initialization events are shown in Fig. 2. Compared with the second harmonic results in Fig. 1, one observes an even stronger centrality dependence on the radial weight power m. For both initializations, for the 0%–5% most central collisions v_3 is best correlated with $\varepsilon_{4,3}$, for the 20%–30% centrality v_3 best correlated with $\varepsilon_{3,3}$, and for the peripheral 50%–60% centrality v_3 best correlated with $\varepsilon_{2,3}$. The choice of $m=2$ for the third harmonic eccentricity, $\varepsilon_{2,3}$, is not very good for central collisions, but is fine for peripheral collisions.

When m in Eq. (3) takes values further away from $m=n$, the event-by-event correlation between v_n and $\varepsilon_{m,n}$ generally becomes worse. One step further away from $m=n$, I set $m=n-2$ and $n+2$, that is, $m=0,4$ for the second harmonic and $m=1,5$ for the third harmonic. The results for the event-by-event correlation between $\varepsilon_{(0,4),2}$ and v_2 and between $\varepsilon_{(1,5),3}$ and v_3 from MC-Glauber and MC-KLN initializations for the 0%–5%, 20%–30%, and 50%–60% collision centralities are shown in Fig. 3.

The event-by-event correlations between $\varepsilon_{(0,4),2}$ and v_2 from MC-Glauber initialization events in Fig. 3 (top left) are indeed worse than those between $\varepsilon_{(1,2,3),2}$ and v_2 in Fig. 1 (left). For the third harmonic, similarly, the event-by-event correlations between $\varepsilon_{(1,5),3}$ and v_3 from MC-Glauber initialization events in Fig. 3 (bottom left) are worse than those between $\varepsilon_{(2,3,4),3}$ and v_3 in Fig. 2 (left). However, there are exceptions. For the

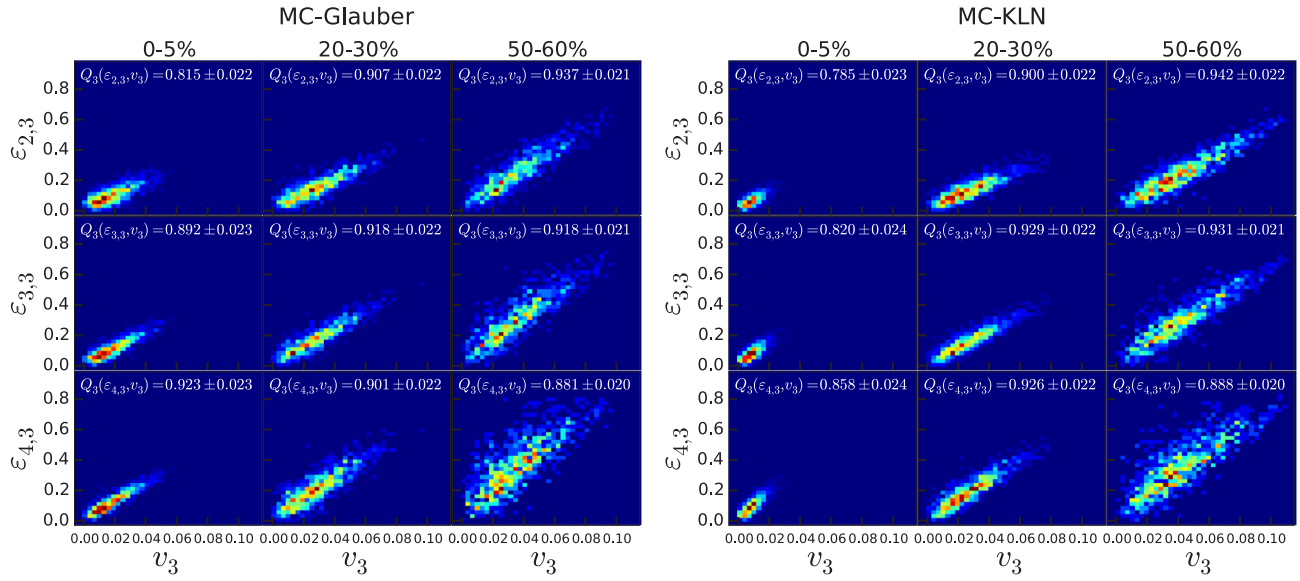

FIG. 2. (Color online) The event-by-event correlations between $\varepsilon_{2,3}$, $\varepsilon_{3,3}$, and $\varepsilon_{4,3}$ and v_3 for the centrality classes 0%–5%, 20%–30%, and 50%–60% with MC-Glauber (left) and MC-KLN (right) initializations.

MC-KLN initialization events, due to the larger shear viscosity strongly damping the small-scale structure, flow coefficients become even more sensitive to eccentricities with larger radial weight power m in the most central collisions, as shown in Fig. 3 (top right and bottom right). For my simulations of MC-KLN initialization events, for the 0%–5% most central

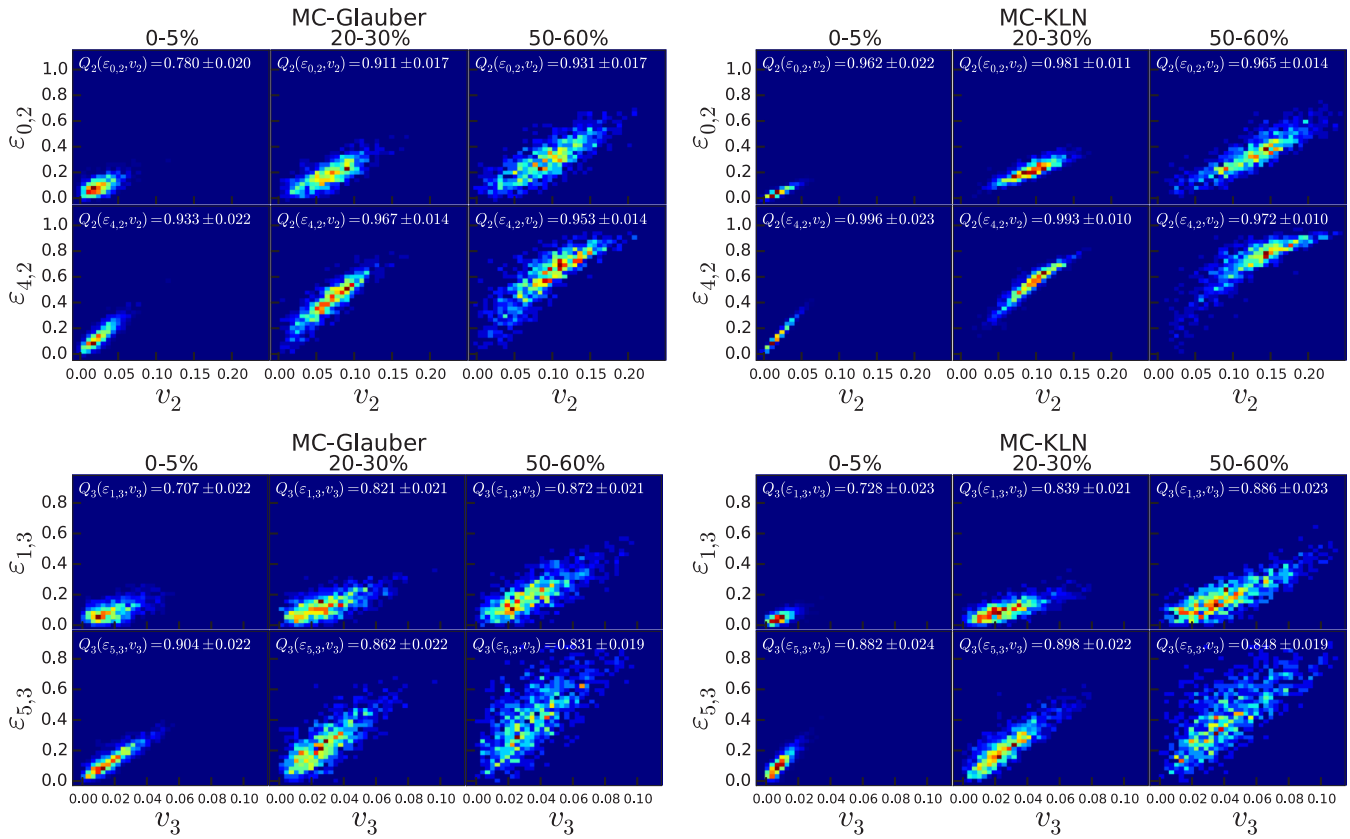

FIG. 3. (Color online) Top panels: The event-by-event correlations between $\varepsilon_{0,2}$ and v_2 and between $\varepsilon_{4,2}$ and v_2 for the centrality classes 0%–5%, 20%–30%, and 50%–60% with MC-Glauber (left) and MC-KLN (right) initializations. Bottom panels: The event-by-event correlations between $\varepsilon_{1,3}$ and v_3 and between $\varepsilon_{5,3}$ and v_3 for the centrality classes 0%–5%, 20%–30%, and 50%–60% with MC-Glauber (left) and MC-KLN (right) initializations.

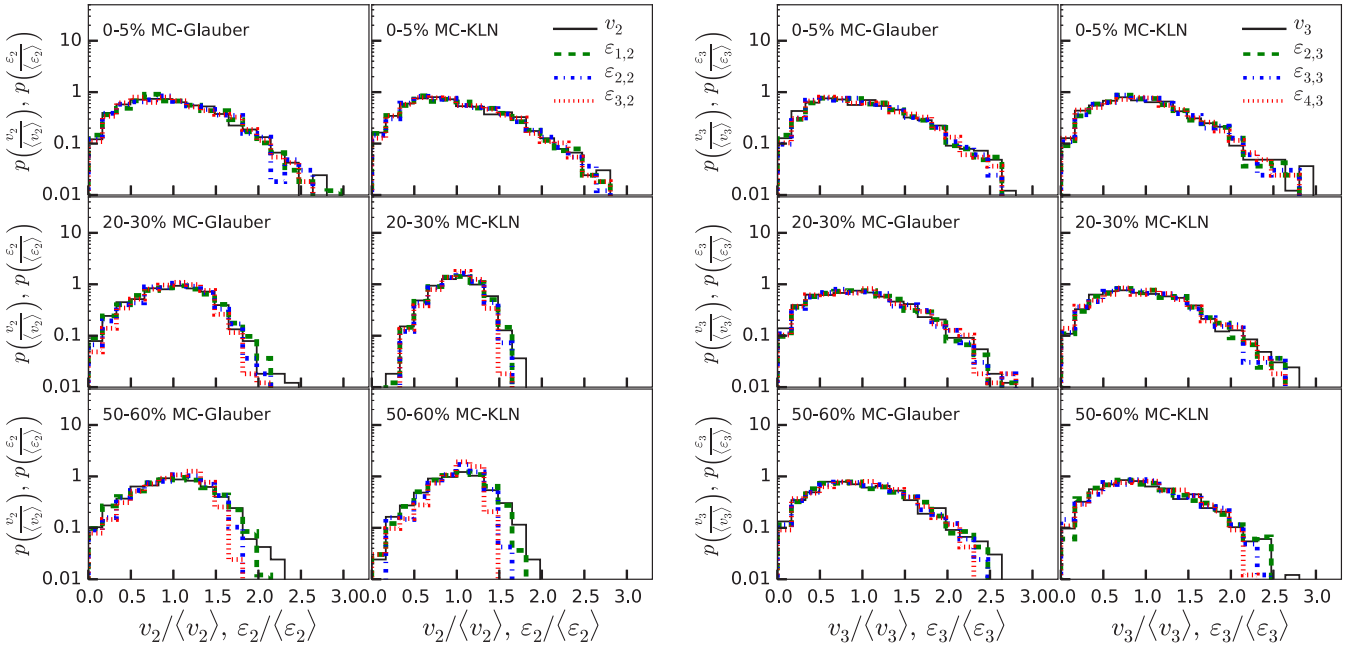

FIG. 4. (Color online) The scaled distributions of the second harmonic eccentricities $\varepsilon_{1,2}$, $\varepsilon_{2,2}$, and $\varepsilon_{3,2}$ and flow v_2 for the centrality classes 0%–5%, 20%–30%, and 50%–60% with MC-Glauber and MC-KLN initializations (left panels). The scaled distributions of the third harmonic eccentricities $\varepsilon_{2,3}$, $\varepsilon_{3,3}$, and $\varepsilon_{4,3}$ and flow v_3 for the centrality classes 0%–5%, 20%–30%, and 50%–60% with MC-Glauber and MC-KLN initializations (right panels).

collisions, up to $m = 6$ the correlation between $\varepsilon_{m,2}$ and v_2 is fairly good, and up to $m = 7$ the correlation between $\varepsilon_{m,3}$ and v_3 is fairly good. Except for the most central collisions with large shear viscosity, the correlations between $\varepsilon_{m,n}$ and v_n become poor when $|m - n| > 2$.

B. Fluctuations

For a more detailed comparison, I study how the full event-by-event distributions of $\varepsilon_{m,n}$ are affected by using different radial weight r^m. To compare the distributions of the initial eccentricities with the final v_n distributions after hydrodynamic evolution, it is convenient to scale the distributions by their respective mean values. The scaled probability distributions of the second harmonic flow $P(\frac{v_2}{\langle v_2\rangle})$ and eccentricities $P(\frac{\varepsilon_{(1,2,3),2}}{\langle\varepsilon_{(1,2,3),2}\rangle})$ for the 0%–5%, 20%–30%, and 50%–60% centrality classes with MC-Glauber and MC-KLN initializations are shown in Fig. 4 (left). Those of the third harmonic flow $P(\frac{v_3}{\langle v_3\rangle})$ and eccentricities $P(\frac{\varepsilon_{(2,3,4),3}}{\langle\varepsilon_{(2,3,4),3}\rangle})$ are shown in Fig. 4 (right).

From Fig. 4 one can see that for the 0%–5% most central collisions, for both the second and third harmonics, the scaled distributions of $\varepsilon_{m,n}$ with different radial weight power m look quite similar, and all have good consistency with the distributions of v_n. For the midcentral 20%–30% centrality class, one starts to see some deviations in the tails of the second harmonic eccentricity distributions. For the peripheral 50%–60% centrality class, the second harmonic eccentricity distributions with different radial weight power m obviously deviate from one another. The second harmonic eccentricity with the largest radial weight power, $\varepsilon_{3,2}$, has the narrowest distribution, while that with the smallest m, $\varepsilon_{1,2}$, has the widest distribution, and the distribution of $\varepsilon_{2,2}$ stays in between them. The probability distribution of v_2 is slightly wider than the initial eccentricity distribution and is most consistent with the distribution of $\varepsilon_{1,2}$. This centrality dependence of the scaled eccentricity distribution on the radial weight power m is the same for both the MC-Glauber and MC-KLN initializations, though the distributions themselves from these two initializations are somewhat different. For the 50%–60% centrality, the third harmonic eccentricity distributions show some deviations similar to those of the second harmonic, but much less in magnitude.

To be more quantitative, the mean values, standard deviations and scaled standard deviations of the second harmonic eccentricities, $\varepsilon_{1,2}$, $\varepsilon_{2,2}$, and $\varepsilon_{3,2}$, as a function of collision centrality are shown in the left-hand panels of Fig. 5, and those of the third harmonic, $\varepsilon_{2,3}$, $\varepsilon_{3,3}$, and $\varepsilon_{4,3}$, are shown in the right-hand panels of Fig. 5. Errors of the data points in Fig. 5 are within the symbols. The mean values of both the second and third harmonic eccentricities (upper panels in Fig. 5) depend on the radial weight power m. Eccentricities with larger m have larger mean values, eccentricities with smaller m have smaller mean values, and the differences between them increase with the collision centrality. The standard deviation of the third harmonic eccentricity [middle panels in Fig. 5 (right)] behaves similarly to the mean value, while the standard deviation of the second harmonic eccentricity [middle panels in Fig. 5 (left)] has a much weaker dependence on the radial weight power m. For peripheral collisions, $\langle\varepsilon_{m,2}\rangle$ increases largely with m, while $\sigma(\varepsilon_{m,2})$ only increases mildly with m. We know that the second harmonic eccentricities $\varepsilon_{m,2}$ measure the initial almond overlapping shape of the colliding nuclei, while the third harmonic eccentricities $\varepsilon_{m,3}$ are caused solely by fluctuations.

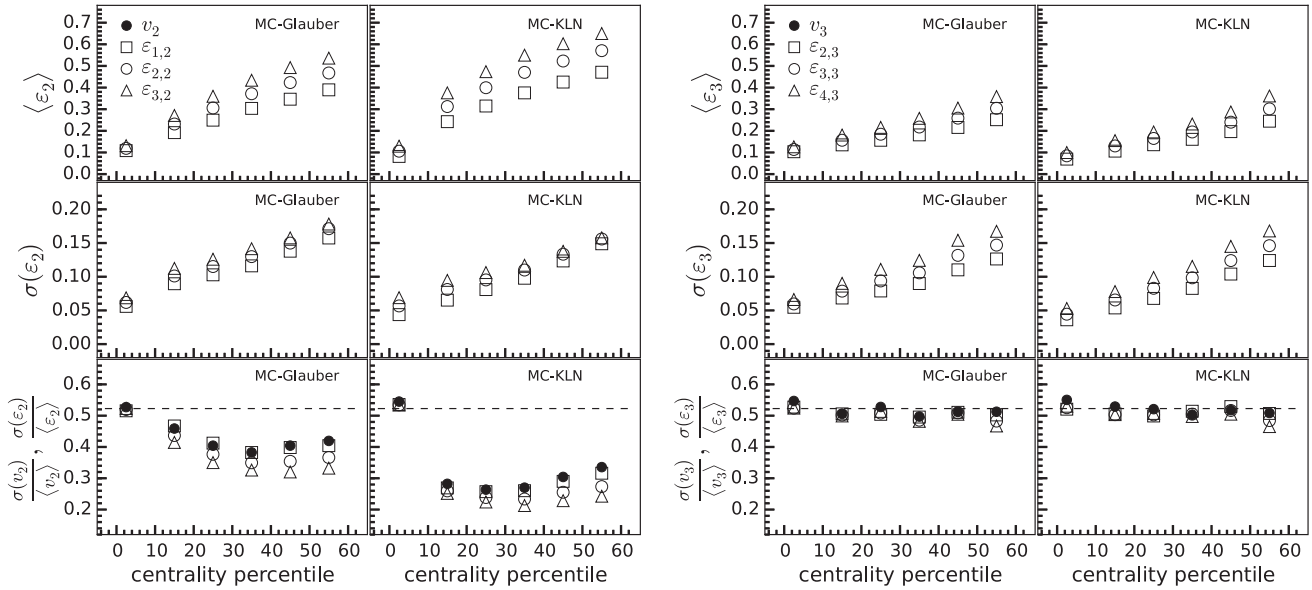

FIG. 5. The mean values, standard deviations, relative standard deviations of $\varepsilon_{1,2}$, $\varepsilon_{2,2}$, and $\varepsilon_{3,2}$, and the relative standard deviation of v_2 as a function of collision centrality for MC-Glauber and MC-KLN initializations (left-hand panels). The mean values, standard deviations, relative standard deviations of $\varepsilon_{2,3}$, $\varepsilon_{3,3}$, and $\varepsilon_{4,3}$, and the relative standard deviation of v_3 as a function of collision centrality for MC-Glauber and MC-KLN initializations (right-hand panels). The dashed lines in the bottom panels indicate the value $\sqrt{4/\pi - 1}$.

This is the reason for the different dependencies of $\sigma(\varepsilon_{m,2})$ and $\sigma(\varepsilon_{m,3})$ on m, as explained in the following subsection.

The scaled standard deviation is the standard deviation divided by the mean value. Because the mean value of the second harmonic eccentricity increases with m much faster than its standard deviation, the scaled standard deviation $\frac{\sigma(\varepsilon_{m,2})}{\langle\varepsilon_{m,2}\rangle}$ decreases with increasing m [lower panels in Figs. 5 (left)]. The dependence of $\frac{\sigma(\varepsilon_{m,2})}{\langle\varepsilon_{m,2}\rangle}$ on m is more obvious for peripheral collisions and is negligible for central collisions. This is consistent with the scaled distributions of $\varepsilon_{m,2}$ in Fig. 4 (left). For the third harmonic, $\langle\varepsilon_{m,3}\rangle$ and $\sigma(\varepsilon_{m,3})$ have similar dependencies on m for all centralities, and their ratios $\frac{\sigma(\varepsilon_{m,3})}{\langle\varepsilon_{m,3}\rangle}$ almost stay constant, as shown in Fig. 5 (right). Also shown in the bottom panels of Fig. 5 are the scaled standard deviations of the flow coefficient v_n after hydrodynamic evolution. For the most central collisions and for the third harmonic, the scaled standard deviations of eccentricities with different radial weight power m all have good consistency with the scaled standard deviations of v_n. For peripheral collisions, the second harmonic eccentricities with smaller radial weight power m have larger scaled standard deviations and better consistency with the scaled standard deviations of v_2.

These results indicate that, in peripheral collisions, if we compare the distributions $p(v_2)$ with $p(\varepsilon_{1,2})$, instead of with $p(\varepsilon_{2,2})$, the additional widening of the v_2 distributions compared with the ε_2 distributions will disappear.

1. Eccentricity distributions

Now we try to understand the reason for the different eccentricity fluctuation behaviors observed for different collision centralities. As we know, both the magnitude and direction of the participant eccentricity $\vec{\varepsilon}_{m,n}$ fluctuate event to event. The simplest parametrization of these fluctuations is a two-dimensional Gaussian probability distribution which, upon integration over the azimuthal angle, yields the Bessel-Gaussian distribution [26,27]:

$$p(\varepsilon_{m,n}) = \frac{\varepsilon_{m,n}}{\sigma^2} I_0\left(\frac{\varepsilon_0 \varepsilon_{m,n}}{\sigma^2}\right) \exp\left(-\frac{\varepsilon_0^2 + \varepsilon_{m,n}^2}{2\sigma^2}\right), \quad (11)$$

where ε_0 is the mean anisotropy in the reaction plane,

$$\varepsilon_0 = -\frac{\int r dr d\phi r^m \cos(n\phi)\rho(r,\phi)}{\int r dr d\phi r^m \rho(r,\phi)},$$

and σ is the typical magnitude of eccentricity fluctuations around this mean anisotropy. For $n = 2$ and $m = 2$, $\varepsilon_0 = \frac{\langle y^2 - x^2\rangle}{\langle y^2 + x^2\rangle}$.

For the most central collisions and for odd harmonics, ε_0 vanishes with symmetry. In this limit, the average $\langle\varepsilon_{m,n}\rangle = \sqrt{\pi/2}\sigma$ and the standard deviation $\sigma(\varepsilon_{m,n}) = \sqrt{2 - \pi/2}\sigma$ [26,27]. Their ratio, $\sigma(\varepsilon_{m,n})/\langle\varepsilon_{m,n}\rangle = \sqrt{4/\pi - 1}$, is approximately a constant, as indicated by the dashed lines in Fig. 5. The scaled distribution of $\varepsilon_{m,n}$ in this limit becomes

$$p\left(\frac{\varepsilon_{m,n}}{\langle\varepsilon_{m,n}\rangle}\right) = \frac{\varepsilon_{m,n}/\langle\varepsilon_{m,n}\rangle}{(\sqrt{2/\pi})^2} \exp\left(-\frac{(\varepsilon_{m,n}/\langle\varepsilon_{m,n}\rangle)^2}{2(\sqrt{2/\pi})^2}\right), \quad (12)$$

which is universal, independent of any parameter. The universality of the scaled eccentricity distributions for the most central collisions and for the third harmonic is observed in Fig. 4. This universality has also been observed in previous publications [15,28].

The distributions of ε_2 in noncentral nucleus-nucleus collisions are better described by the elliptic power

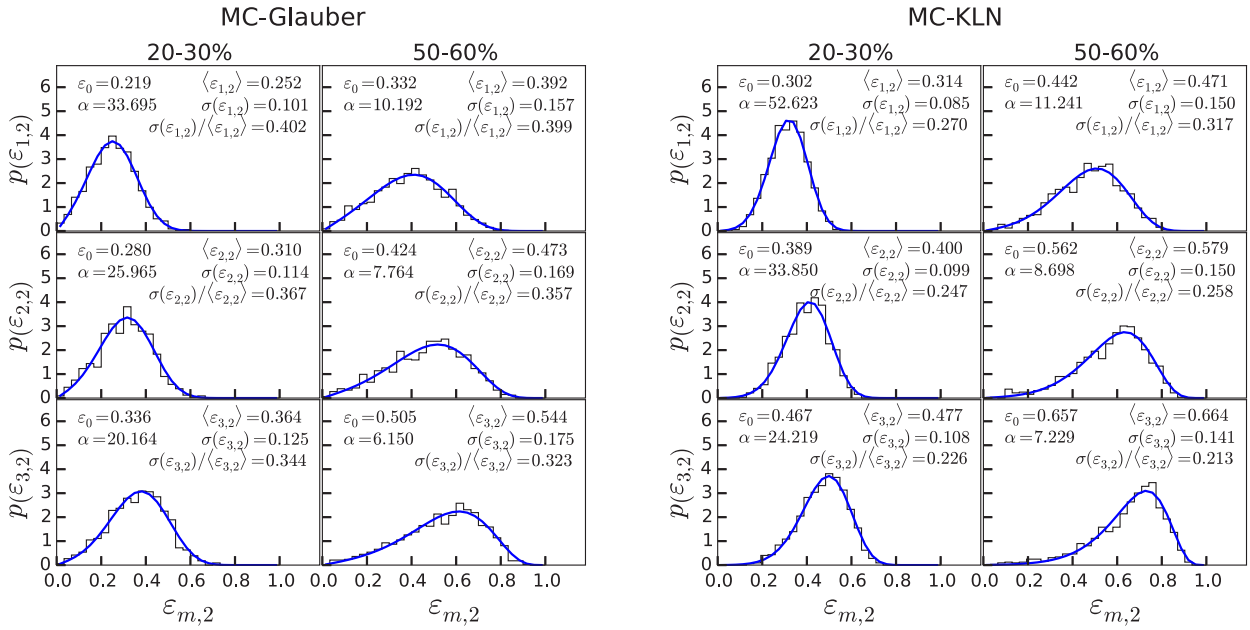

FIG. 6. (Color online) Elliptic power fits of the $\varepsilon_{1,2}$, $\varepsilon_{2,2}$, and $\varepsilon_{3,2}$ distributions in 20%–30% and 50%–60% centrality bins with MC-Glauber (left) and MC-KLN (right) initializations.

distribution [29]:

$$p(\varepsilon_{m,n}) = \frac{\alpha\varepsilon_{m,n}}{\pi}\left(1-\varepsilon_0^2\right)^{\alpha+\frac{1}{2}} \int_0^{2\pi} \frac{\left(1-\varepsilon_{m,n}^2\right)^{\alpha-1} d\phi}{\left(1-\varepsilon_0\varepsilon_{m,n}\cos\phi\right)^{2\alpha+1}}, \tag{13}$$

where ε_0 is the same as in Eq. (11) and α describes the fluctuations. Elliptic power fits of the $\varepsilon_{1,2}$, $\varepsilon_{2,2}$, and $\varepsilon_{3,2}$ distributions in 20%–30% and 50%–60% centrality bins with MC-Glauber and MC-KLN initializations are presented in Fig. 6. The mean and the standard deviation of the elliptic power distribution need to be calculated numerically as a function of ε_0 and α. The results of $\langle\varepsilon_{m,2}\rangle$, $\sigma(\varepsilon_{m,2})$, and $\sigma(\varepsilon_{m,2})/\langle\varepsilon_{m,n2}\rangle$, together with the fitting parameters ε_0 and α, are listed in Fig. 6. The scaled standard deviation $\sigma(\varepsilon_{m,2})/\langle\varepsilon_{m,2}\rangle$ from the elliptic power distribution decreases as the radial weight power m increases, closely matching the Monte Carlo results in Fig. 5.

The small deviation in the tail of the $p(\varepsilon_{m,3})$ distributions for the 50%–60% centrality bin in Fig. 4 (right) is due to the nonzero correlation between ε_2 and ε_3 when the collision centrality is larger than 50% [30].

2. *Hadronic rescattering*

Hadronic rescattering generally modifies the flow coefficient and its probability distribution. To study this effect, hadrons produced on the particalization hypersurface are converted into an initial condition file for the hadronic rescattering model Ultrarelativistic Quantum Molecular Dynamics (UrQMD) to calculate the further evolution of the hadrons [5]. UrQMD is a microscopic transport model and has been extensively used to model the evolution of hadronic systems [31]. The results of scaled v_2 distributions before and after hadronic rescattering for the centrality classes 0%–5%, 20%–30%, and 50%–60% are shown in Fig. 7. The values of the scaled standard deviations, $\frac{\sigma(v_2)}{\langle v_2\rangle}$, with statistical errors are listed.

For the 0%–5% most central collisions, the scaled v_2 probability distributions before and after hadronic rescattering

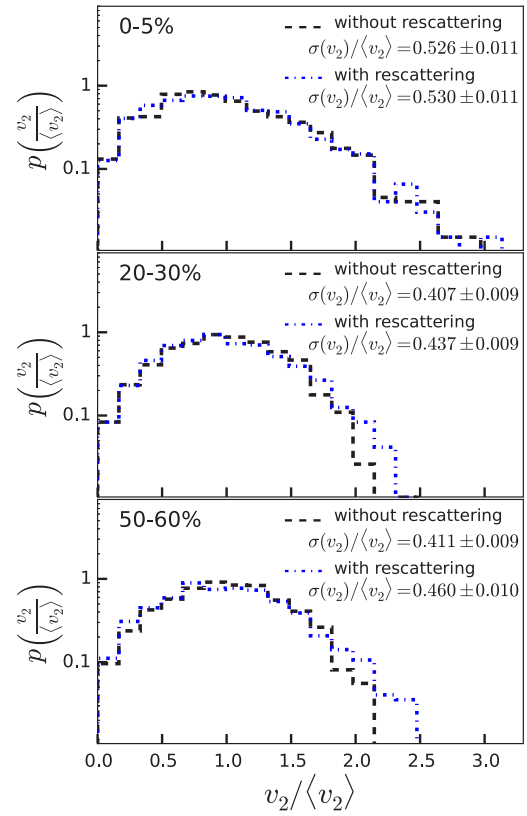

FIG. 7. (Color online) The scaled v_2 distributions before and after hadronic rescattering for the centrality classes 0%–5%, 20%–30%, and 50%–60% with MC-Glauber initialization.

nicely agree with each other and can be described by the universal expression Eq. (12), following the corresponding initial eccentricity probability distribution. Their scaled standard deviations, $\frac{\sigma(v_2)}{\langle v_2\rangle}$, approach the limiting value $\sqrt{4/\pi - 1}$. For noncentral collisions, the scaled v_2 distributions with hadronic rescattering are wider than those without. Hadronic rescattering increases the scaled standard deviation of the v_2 distribution, and this increase is more obvious for the more peripheral collisions. Results in Fig. 7 are from the MC-Glauber initialization, those from the MC-KLN initialization are similar and not shown. The probability distributions of the third harmonic flow coefficient v_3 before and after hadronic transport are consistent with each other, similar to the v_2 distributions in the most central collisions.

These results indicate that hadronic rescattering contributes to the widening of the $p(v_2)$ distribution compared with the $p(\varepsilon_2)$ distribution in peripheral collisions. The magnitude of the increase of $\frac{\sigma(v_2)}{\langle v_2\rangle}$ when including hadronic transport is of the same order as the difference between $\frac{\sigma(\varepsilon_{m,2})}{\langle \varepsilon_{m,2}\rangle}$ when defined with different m.

IV. CONCLUSIONS

In this work, the correlations between the flow coefficient v_n and the initial eccentricity $\varepsilon_{m,n}$ in ultrarelativistic heavy-ion collisions have been studied using event-by-event hydrodynamics. The radial weight power m of $\varepsilon_{m,n}$ has been set to values around $m = n$, mainly $m = n - 1$, n, and $n + 1$, to study the dependence on m. The results show that, for the second and third harmonics, the event-by-event correlation between v_n and $\varepsilon_{m,n}$ depends on the collision centrality and the fluid viscosity. Generally, for the more central collisions, v_n is better correlated with $\varepsilon_{m,n}$ defined with relatively larger m, like $\varepsilon_{n+1,n}$, while for the more peripheral collisions, v_n is better correlated with $\varepsilon_{m,n}$ with relatively smaller m, like $\varepsilon_{n-1,n}$. Large fluid viscosity leads to v_n more sensitive to $\varepsilon_{m,n}$ with $m > n$ in central collisions.

For the most central collisions and for odd harmonics, anisotropy is solely due to fluctuations, and eccentricity distributions can be described by the Gaussian distribution. In this case, the scaled probability distributions of $\varepsilon_{m,n}$ are universal and have good consistency with the scaled flow coefficient v_n distributions. For noncentral collisions, the second harmonic eccentricity distributions are better described by the elliptic power distribution, which leads to the scaled probability distributions of $\varepsilon_{m,2}$ with different radial weight power m deviating from one another, and the deviation increases with the collision centrality. In peripheral collisions, $\varepsilon_{m,2}$ with smaller m has a wider scaled probability distribution and a larger scaled standard deviation, and better consistency with the scaled v_2 distribution after hydrodynamic evolution. Including hadronic rescattering further widens the scaled v_2 distribution in noncentral collisions. Both the dependence of $p(\varepsilon_{m,2})$ distribution on m and hadronic rescattering contribute to the observed inconsistency between $p(v_2)$ and $p(\varepsilon_2)$ distributions.

If future analysis of the event-by-event flow distributions include the centrality-dependent weight factors for the eccentricities, this might lead to better agreement with the experimental data and improve the understanding of the current issues with the centrality dependence in a single specific initial state model. The residual inconsistency between $p(v_2)$ and $p(\varepsilon_{m,2})$ distributions is mainly due to hadronic rescattering.

ACKNOWLEDGMENTS

The author acknowledges the support of the FANEDD of the People's Republic of China under Project No. 200523 and the NNSFC under Projects No. 10305004 and No. 11221504.

[1] U. Heinz and R. Snellings, Annu. Rev. Nucl. Part. Sci. **63**, 123 (2013).
[2] M. Luzum and H. Petersen, J. Phys. G **41**, 063102 (2014).
[3] M. Gyulassy and L. McLerran, Nucl. Phys. A **750**, 30 (2005).
[4] S. Voloshin and Y. Zhang, Z. Phys. C **70**, 665 (1996).
[5] C. Shen, Z. Qiu, H. Song, J. Bernhard, S. Bass, and U. Heinz, arXiv:1409.8164 [nucl-th].
[6] C. Gale, S. Jeon, and B. Schenke, Int. J. Mod. Phys. A **28**, 1340011 (2013).
[7] H. Sorge, Phys. Rev. Lett. **82**, 2048 (1999).
[8] B. Alver*et al.* (PHOBOS Collaboration), Phys. Rev. Lett. **98**, 242302 (2007).
[9] B. Alver and G. Roland, Phys. Rev. C **81**, 054905 (2010).
[10] D. Teaney and L. Yan, Phys. Rev. C **83**, 064904 (2011).
[11] F. G. Gardim, F. Grassi, M. Luzum, and J.-Y. Ollitrault, Phys. Rev. C **85**, 024908 (2012).
[12] C. E. Coleman-Smith, H. Petersen, and R. L. Wolpert, J. Phys. G **40**, 095103 (2013).
[13] S. Floerchinger and U. A. Wiedemann, Phys. Rev. C **88**, 044906 (2013).
[14] J. Jia, J. Phys. G **41**, 124003 (2014).
[15] G. Aad *et al.* (ATLAS Collaboration), J. High Energy Phys. 11 (2013) 183.
[16] L. Yan, J.-Y. Ollitrault, and A. M. Poskanzer, Phys. Lett. B **742**, 290 (2015).
[17] R. Snellings *et al.* (ALICE Collaboration), J. Phys. G **38**, 124013 (2011).
[18] C. Gale, S. Jeon, B. Schenke, P. Tribedy, and R. Venugopalan, Nucl. Phys. A **904**, 409c (2013).
[19] H. Niemi, Nucl. Phys. A **931**, 227 (2014).
[20] A. Adil, H. J. Drescher, A. Dumitru, A. Hayashigaki, and Y. Nara, Phys. Rev. C **74**, 044905 (2006).
[21] Z. Qiu, C. Shen, and U. Heinz, Phys. Lett. B **707**, 151 (2012).
[22] P. Huovinen and P. Petreczky, Phys. Rev. D **10**, 186 (1974).
[23] F. Cooper and G. Frye, Nucl. Phys. A **837**, 26 (2010).
[24] H. Niemi, G. S. Denicol, H. Holopainen, and P. Huovinen, Phys. Rev. C **87**, 054901 (2013).
[25] F. G. Gardim, J. Noronha-Hostler, M. Luzum, and F. Grassi, Phys. Rev. C **91**, 034902 (2015).

[26] S. A. Voloshin, A. M. Poskanzer, A. Tang, and G. Wang, Phys. Lett. B **659**, 537 (2008).
[27] W. Broniowski, P. Bożek, and M. Rybczyński, Phys. Rev. C **76**, 054905 (2007).
[28] T. Renk and H. Niemi, Phys. Rev. C **89**, 064907 (2014).
[29] L. Yan, J.-Y. Ollitrault, and A. M. Poskanzer, Phys. Rev. C **90**, 024903 (2014).
[30] J. L. Nagle and M. P. McCumber, Phys. Rev. C **83**, 044908 (2011).
[31] S. Bass, M. Belkacem, M. Bleicher, M. Brandstetter, L. Bravina *et al.*, Prog. Part. Nucl. Phys. **41**, 255 (1998).